Speckle contrast diffuse correlation tomography of complex turbid medium flow

Chong Huang, Daniel Irwin, Yu Lin, Yu Shang, Lian He, Weikai Kong, Jia Luo, and Guoqiang Yu

Articles you may be interested in

Three-dimensional flow contrast imaging of deep tissue using noncontact diffuse correlation tomography
Appl. Phys. Lett. **104**, 121103 (2014); 10.1063/1.4869469

Three-dimensional fluorescence-enhanced optical tomography using a hand-held probe based imaging system
Med. Phys. **35**, 3354 (2008); 10.1118/1.2940603

Fully adaptive FEM based fluorescence optical tomography from time-dependent measurements with area illumination and detection
Med. Phys. **33**, 1299 (2006); 10.1118/1.2190330

Three-dimensional fluorescence lifetime tomography
Med. Phys. **32**, 992 (2005); 10.1118/1.1861160

Magnetic resonance-guided near-infrared tomography of the breast
Rev. Sci. Instrum. **75**, 5262 (2004); 10.1063/1.1819634

Medical Physics Letter

Speckle contrast diffuse correlation tomography of complex turbid medium flow

Chong Huang,[a)] Daniel Irwin,[a)] Yu Lin, Yu Shang, Lian He, and Weikai Kong
Department of Biomedical Engineering, University of Kentucky, Lexington, Kentucky 40506

Jia Luo
Department of Pharmacology and Nutritional Sciences, University of Kentucky, Lexington, Kentucky 40506

Guoqiang Yu[b)]
Department of Biomedical Engineering, University of Kentucky, Lexington, Kentucky 40506

Purpose: Developed herein is a three-dimensional (3D) flow contrast imaging system leveraging advancements in the extension of laser speckle contrast imaging theories to deep tissues along with our recently developed finite-element diffuse correlation tomography (DCT) reconstruction scheme. This technique, termed speckle contrast diffuse correlation tomography (scDCT), enables incorporation of complex optical property heterogeneities and sample boundaries. When combined with a reflectance-based design, this system facilitates a rapid segue into flow contrast imaging of larger, *in vivo* applications such as humans.

Methods: A highly sensitive CCD camera was integrated into a reflectance-based optical system. Four long-coherence laser source positions were coupled to an optical switch for sequencing of tomographic data acquisition providing multiple projections through the sample. This system was investigated through incorporation of liquid and solid tissue-like phantoms exhibiting optical properties and flow characteristics typical of human tissues. Computer simulations were also performed for comparisons. A uniquely encountered smear correction algorithm was employed to correct point-source illumination contributions during image capture with the frame-transfer CCD and reflectance setup.

Results: Measurements with scDCT on a homogeneous liquid phantom showed that speckle contrast-based deep flow indices were within 12% of those from standard DCT. Inclusion of a solid phantom submerged below the liquid phantom surface allowed for heterogeneity detection and validation. The heterogeneity was identified successfully by reconstructed 3D flow contrast tomography with scDCT. The heterogeneity center and dimensions and averaged relative flow (within 3%) and localization were in agreement with actuality and computer simulations, respectively.

Conclusions: A custom cost-effective CCD-based reflectance 3D flow imaging system demonstrated rapid acquisition of dense boundary data and, with further studies, a high potential for translatability to real tissues with arbitrary boundaries. A requisite correction was also found for measurements in the fashion of scDCT to recover accurate speckle contrast of deep tissues. © *2015 American Association of Physicists in Medicine.* [http://dx.doi.org/10.1118/1.4922206]

1. INTRODUCTION

Near-infrared (NIR) light enables the deep tissue investigation of microvascular hemodynamics.[1,2] Blood flow is one such available observable promoting a wealth of physiological insight both individually and in combination with other metrics. Diffuse correlation spectroscopy (DCS) and, to a lesser extent, tomography (DCT) have received interest over the past two decades as noninvasive methods for blood flow recovery.[3,4] In typical DCS implementations, the temporal fluctuations in individual speckles are measured by avalanche photodiodes (APDs) coupled to independent optical fibers. These impose a physical and monetary overhead limiting the potential sampling density and temporal resolution. In our previous work, we extended DCS into a noncontact lens-based system succeeded by noncontact DCT (ncDCT) within a finite element method (FEM) framework.[1,5] These studies provided desirable operational attributes, especially the elimination of hemodynamic alterations due to contact compression and the ability to incorporate arbitrary tissue boundaries and compositions. Moreover, our FEM reconstruction method is based on readily available open source software for

seamless integration of geometries and inversion algorithm techniques.[6] The mechanical scanning of an optical fiber array in ncDCT to cover a region of interest (ROI) provides one solution to increasing sampling density and reducing cost, but increases measurement duration and may introduce motion artifacts. Another solution we outline here, recruitment of charge-coupled device (CCD) detection, promotes advantages including increased sampling density, decreased sampling times and equipment overhead, and geometry extraction potential.

CCD detection has frequently been utilized successfully in other flow monitoring techniques such as laser speckle contrast imaging.[7] This modality applies a wide-field illuminating source to enable rapid collection of two-dimensional images depicting spatial vessel flow variations on superficial tissues. There have been a few recent advancements toward blood flow monitoring in deep tissue with NIR point-source illumination and CCD detection. Diffuse speckle contrast analysis and speckle contrast optical spectroscopy approach the problem by using the relationship between a speckle contrast parameter and DCS theory.[8,9] Speckle contrast optical tomography (SCOT) extends the concept using an analytical Born approximation in the inverse problem on transmission-based measurement of parallel-plane tissue phantoms.[10]

We move forward from these studies in the direction of tomographic imaging by developing a robust technique combining the benefits of CCD detection and our FEM-based DCT flow reconstruction. In contrast to SCOT which formulates the inverse problem with a direct analytical relationship between the speckle contrast and mean-square-displacement of moving scatterers, we simplify the process by converting the speckle contrast to boundary flow indices and retaining our leverage of FEM-based DOT reconstruction advancements. Specifically, in this study we are able to take advantage of the nonlinear iterative algorithms, finite-element support functions, data filtering, and the many features included in the modified NIRFAST for DCT.[5] This is due to the formal similarity between DOT and DCT as outlined in our previous publication.[5] This unique method, termed speckle contrast DCT (scDCT), facilitates three-dimensional (3D) flow contrast imaging of complex turbid media. As this technique promotes incorporation of both heterogeneous optical properties and arbitrary tissue boundaries, scDCT can utilize highly representative sample characteristics in the recovery of accurate flow data. We apply this scDCT technique on a reflectance-based measurement which more adequately represents the situation encountered in larger subjects such as humans where transmission is not practical in most cases (due to the limited penetration depth of light), enhancing translatability. A smear correction algorithm is also incorporated in this study to resolve the influences on data uniquely incurred when using frame-transfer CCDs with the point-source illumination and reflectance setup.

2. METHODS AND MATERIALS

As shown in Fig. 1(a), the scDCT equipment and experimental setup involve a 785 nm long coherence laser (coherence

length >5 m, CrystaLaser, NV) to emit photons into the sample. A fiber optic switch (VX500, Dicon, CA) with four-channel outputs delivered photons to four multimode optical fibers (FT200UMT, Thorlabs, NJ) individually. The fibers [S1–S4 in Fig. 1(b)] were located 1.5 cm from the field of view (FOV) edge centers. An electron-multiplying CCD (EMCCD; Cascade 1K, Photometrics, AZ) with a zoom lens (Zoom 7000, Navitar, NY) aligned concentrically to the FOV detected the speckle patterns due to the diffused light. The focal length of the image lens was 35 mm, making the focal plane on the surface of the liquid phantom. An F number of 8 was chosen to ensure the speckle size satisfied the Nyquist sampling criteria.[11]

In DCS theory, the unnormalized electric field temporal autocorrelation function, $G_1(\mathbf{r},\tau) = \langle E(\mathbf{r},t)E^*(\mathbf{r},t+\tau)\rangle$, is observed to propagate diffusely according to the following correlation diffusion equation (CDE) in biological tissues:[3]

$$\nabla \cdot \left(\left(\frac{D(\mathbf{r})}{v}\right) \nabla G_1(\mathbf{r},\tau) \right)$$
$$- \left(\mu_a(\mathbf{r}) + \frac{1}{3}\mu_s'(\mathbf{r})k_0^2\alpha\langle \Delta r^2(\tau)\rangle \right) G_1(\mathbf{r},\tau)$$
$$= -S(\mathbf{r})\exp\left(i\left(\frac{2\pi\tau c}{\lambda}\right)\right), \tag{1}$$

with position vector $\mathbf{r}$, tissue absorption $\mu_a(\mathbf{r})$, reduced scattering $\mu_s'(\mathbf{r})$, and photon diffusion $D(\mathbf{r}) \approx v/3\mu_s'(\mathbf{r})$ coefficients, wavenumber k_0, speed of light in vacuum c, light speed in tissue v, wavelength λ, correlation delay time τ, and source term $S(\mathbf{r})$ as a point source in this study. The mean-square-displacement of dynamic scatterers (e.g., red blood cells) in autocorrelation delay time τ is denoted by $\langle \Delta r^2(\tau)\rangle$. For the case of diffuse motion this can be modeled by $6D_B(\mathbf{r})\tau$, with $D_B(\mathbf{r})$ denoting the heterogeneous effective diffusion coefficient. A unitless factor α accounts for the moving to static scatterer ratio and combines to produce a blood flow index (BFI) as $\alpha D_B(\mathbf{r})$. In our homogeneous liquid phantom experimentation, all scatterers are dynamic ($\alpha = 1$) and we thus write D_B. The CDE analytic solution for semi-infinite homogeneous media used herein establishes the form of the normalized G_1 defined by $g_1(\mathbf{r},\tau) = G_1(\mathbf{r},\tau)/G_1(\mathbf{r},0)$ and has been shown elsewhere.[2]

For a certain CCD camera exposure time, T, the speckle contrast, K, is defined as the ratio of the standard deviation, σ, to mean, μ, intensities across pixels in a chosen window, i.e., $K = \sigma/\mu$. Using the Siegert relationship, this spatial speckle contrast parameter can be related to the temporal correlation function g_1 by[12]

$$K^2 = \frac{2\beta}{T} \int_0^T (1-\tau/T)[g_1(\mathbf{r},\tau)]^2 d\tau, \tag{2}$$

where β relates detector and speckle size. We substitute in the form of g_1 from the analytical solution to Eq. (1) for semi-infinite geometry and find a nonlinear relationship between speckle contrast and BFI, i.e., $K^2 = f(\alpha D_B,T,\mu_a,\mu_s',\lambda,\beta,S - D,k_0)$ where $S - D$ is source-detector separation.[8] We then minimize the squared difference between the experimentally measured speckle contrast and theoretical result, $(K^2 - f)^2$,
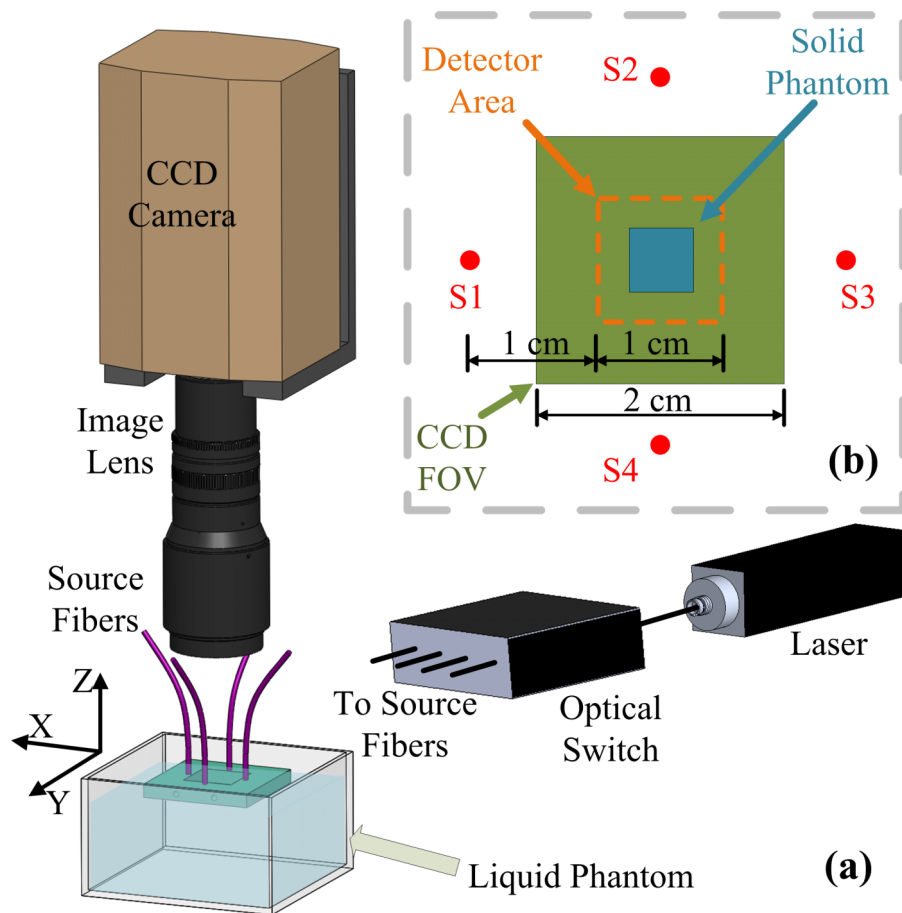
FIG. 1. (a) The EMCCD is focused onto a liquid phantom surface. A square metal holder positioned four fibers supporting their ferrule tips on the liquid surface. The holder provided a 2.4×2.4 cm open area. The optical switch distributed laser light into the four source fibers sequentially. (b) Configuration of the four sources, CCD FOV, solid phantom placement, and detector area.

with respect to the BFI. These calculated BFIs are then representative of the boundary measurements for insertion into the modified NIRFAST program as developed previously for flow contrast reconstructions.[5,6]

Briefly, for tomography we begin by populating the normalized semi-infinite solution to Eq. (1), $g_1(\mathbf{r},\tau)$, with the calculated boundary BFI measurements, known parameters, and a single delay time[5] $\tau = 3.2 \times 10^{-6}$ s. The $S - D$ separation is determined for each effective detector as the center of the region covered by its associated pixels. This set of information is combined with the forward solution from NIRFAST [i.e., $G_1(\mathbf{r},0)$] using a homogeneous mesh to obtain boundary $G_1(\mathbf{r},\tau) = G_1(\mathbf{r},0) \times g_1(\mathbf{r},\tau)$. The absorption coefficient is combined with a dynamic absorption coefficient defined by $\mu_a^d(\mathbf{r},\tau) = 2\mu_s'(\mathbf{r})k_0^2\alpha D_B(\mathbf{r})\tau$. Initially, the latter is determined using a measured or assumed background BFI. Reconstructions of the combined term, $\mu_a(\mathbf{r}) + \mu_a^d(\mathbf{r},\tau)$, are then carried out in NIRFAST using the "Standard" options for a single wavelength and continuous-wave application. A median filter built into NIRFAST is used for phantom test reconstructions as it assists in stabilizing inherent experimental noise. This is because in real measurements the inverse problem is likely to generate odd solutions in a few nodes which may not be encountered with ideal simulation.[5,6] The median filter offers six-level smoothing

from none to high (0–5) and we select level 2 in this study. The inverse problem is set up using modified-Tikhonov regularization with minimization with respect to optical properties and a biconjugate gradient stabilized iterative inversion scheme for Jacobian construction, as implemented in NIRFAST.[6] The BFIs are then extracted from the reconstructed combined absorption coefficient using its definition above.

The speckle contrast obtained from a frame-transfer EM-CCD camera may be deviated from the theoretical presence by intensity disorder from the frame transfer process.[13] More specifically, visual stripes (smears) are induced extending from bright features in the image into the direction opposite that of the charge-transfer process. Along this direction, the smear can be corrected using an algorithm described by Eq. (3). The actual pixel intensity signal of the xth column and yth row $i(x,y)$ can be restored by the measured value $i'(x,y)$ with

$$i(x,y) = i'(x,y) - \frac{\eta t_{ft}}{n_p T} \sum_{n=1}^{y-1} i(x,n), \qquad (3)$$

where t_{ft} is frame transfer time, n_p is number of pixel rows when the frame has moved to the readout buffer, and η is the efficiency with which photoelectrons are generated during

the charge-transfer process relative to the efficiency with which photoelectrons are generated during the image capture period. Our EMCCD frame transfer time is ~1 ms. We set 7×7 windows at the same distance to the source location for a symmetric intensity distribution, leading to η value of 0.67.

Preprocessing of raw EMCCD images is required as follows. Speckle contrast contributions due to hardware noise (i.e., shot noise and dark noise) are accounted for correcting the speckle contrast computation, $K_{\mathrm{meas}} = (\sigma/\mu)$, of windowed regions.[9,14] Details of these corrections can be found elsewhere.[9] Briefly, dark images are used to mitigate speckle contrast influences from dark noise, $I_c = I - I_D$, where I is the original intensity of a single pixel and I_D is the intensity of dark current. The shot noise of I_C follows Poisson statistics, $\sigma_s(I_C) = \sqrt{\mu(I_C)}$, which are incorporated into the correction calculation. The shot and dark corrected speckle contrast is then given by

$$K = \sqrt{\frac{\sigma^2(I) - \sigma^2(I_D) - \sigma_s^2(I_C)}{\mu^2(I_C)}}. \qquad (4)$$

For physical experimentation, a liquid phantom provided a homogeneous tissue-like model by a mixture of distilled water, India ink (Black India, MA), and Intralipid (Fresenius Kabi, Sweden).[15] The property of real tissue was mimicked by setting $\mu_a = 0.05$ cm^{-1}, $\mu_s' = 7.0$ cm^{-1}, and $D_B \cong 1 \times 10^{-8}$ cm^2/s (assumed[15]). A cube-shaped solid phantom ($\mu_a = 0.05$ cm^{-1}, $\mu_s' = 7.0$ cm^{-1}, and αD_B, was measured by DCS to be about three orders of magnitude lower than the liquid background) of carbon black, titanium dioxide, silicone with 7 mm side length was submerged to a 2 mm depth beneath the surface of the FOV center.

3. RESULTS AND DISCUSSION

During both heterogeneity presence and absence experiments, the scDCT measurement protocol consisted of speckle contrast recovery over the liquid surface in a sequential manner for each of the four sources. For each source, 30 frames were acquired with an exposure time of 2 ms and frame rate of 8 frames/s. We defined 9×9 detectors centered in the FOV over 1.0×1.0 cm [Fig. 1(b)] surrounding the target surface. The resulting $S - D$ separations were all 1.0–2.0 cm with 1.25 mm distance between detectors. Each detector (0.42×0.42 mm) included 3×3 windows and each window contained 7×7 pixels (8 μm pixel size). Measured speckle contrast was calculated per window and averaged across those corresponding to their associated detector. Localized speckle contrast averages were then calculated along obtained frames.

The homogeneous phantom was measured with scDCT first in the manner just described, followed by a standard DCS measurement for calibration purposes. Practically, the optical constant β is not available for measurement. A calibration factor was thus determined which equals to the ratio between speckle contrasts from scDCT and those calculated using Eq. (2) with the semi-infinite CDE analytical
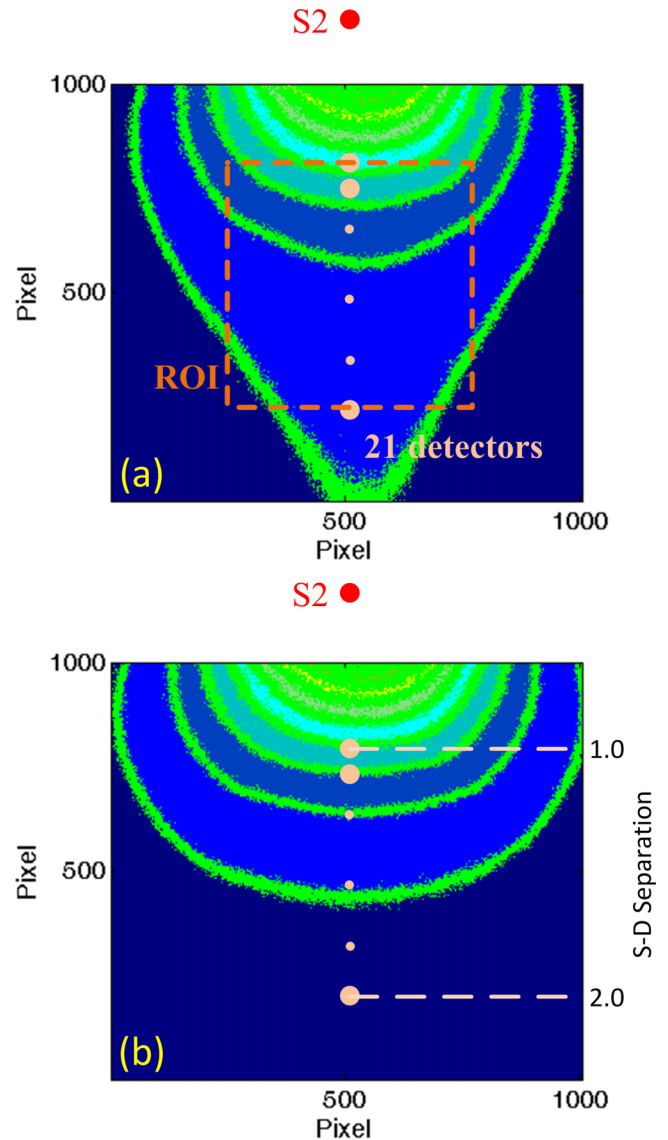

FIG. 2. (a) Original intensity pattern for source S2 on the homogeneous phantom. (b) Desmeared intensity distribution of (a) with a corresponding $S - D$ separation axis. These images depict contours of the intensity profiles with dots representing 21 effective detectors for demonstrating the K distribution with the $S - D$ separations. Note that the dots are not to scale and the smaller dots serve as an ellipsis for the intermediate detectors.

solution for g_1 along with DCS ($\beta = 0.5$) measured BFI on the homogeneous phantom.

Figure 2(a) illustrates the intensity distribution with source S2 on the homogeneous phantom. Figure 2(b) shows the distribution after desmearing, demonstrating a normal presentation for point-source intensity. To quantify the desmearing influence, we consider an array of detectors defined along the center row in line with the source location as shown relative to S2 in Fig. 2(a). The $S - D$ ranges from 1.0 to 2.0 cm. For each remaining source the detectors are defined similarly, but with different orientation based on the source location. The measured K for such detectors and each source with and without desmearing is shown in Fig. 3(a), along with the calculated K. To refine this depiction, we increased effective detectors along the center row to 21
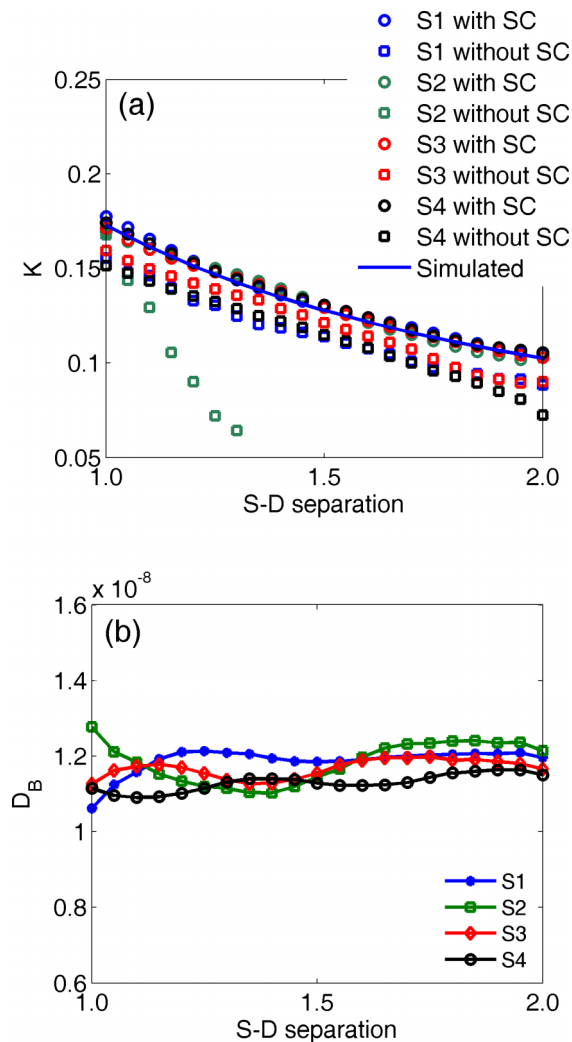
FIG. 4. Measured speckle contrast distributions from S1 on homogeneous and heterogeneous phantoms.

FIG. 3. (a) K for all sources from detectors defined along the center row with and without smear correction (SC) and numerically simulated K at the $S-D$ separations. (b) D_B for center row detectors.

[see the ROI and dots in Fig. 2(a)] while defining them the same way as done elsewhere in the experimentation. It can be seen that the desmeared K correlates with the calculation. The region of usable speckle contrast without desmearing is obviously limited with S2 most noticeably impacted. This is due to our system configuration in which frame transfer occurs in the direction from S2 to S4. The D_B value across the center row of detectors is shown in Fig. 3(b). The D_B value achieved from DCS at 2.0 cm $S-D$ separation was 1.28×10^{-8} cm^2/s. The independently averaged D_B for S1–S4 at the 21 detectors were $(1.19 \pm 0.05) \times 10^{-8}$ cm^2/s, $(1.18 \pm 0.08) \times 10^{-8}$ cm^2/s, $(1.17 \pm 0.06) \times 10^{-8}$ cm^2/s, and $(1.13 \pm 0.06) \times 10^{-8}$ cm^2/s. These are in good agreement (within 12%) with the standard DCS measurement. The comparison of K distributions measured from S1 on the homogeneous and heterogeneous phantoms is shown in Fig. 4.

Next, we measured speckle contrast in the phantom with heterogeneity. The corresponding boundary BFIs were combined with the BFI obtained from the homogeneous phantom measurements for image reconstructions. We used a finite
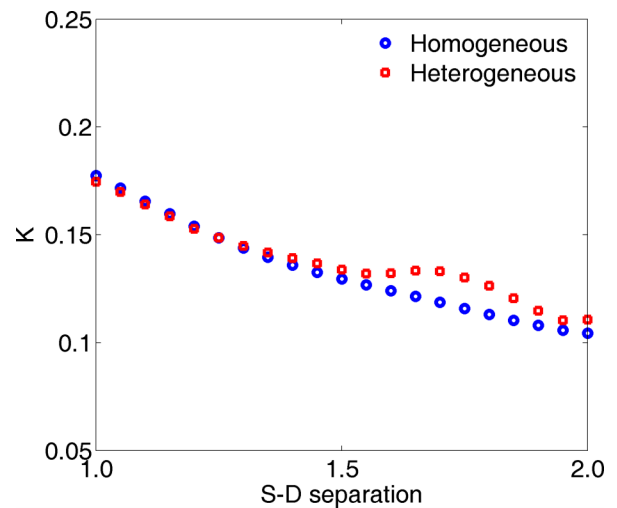
element mesh [dimension(mm): $60(H) \times 60(W) \times 30(D)$] centered at (0,0,15) with a 3 mm node distance.[5] The mesh was refined in the known region of heterogeneity to improve detection resolution while not overwhelmingly increasing the number of nodes. Refinement was within a 15 mm radius (e.g., inclusive of five elements) centered from (0,0,30) to a 1.5 mm node distance (total nodes: 10 307) using ANSYS® (ANSYS, PA). The relative blood flow, rBF, is used to denote the ratio of phantom with heterogeneity to homogeneous phantom αD_B's. As presented in our previous work,[5] the algorithm based on an open software package NIRFAST[6] was used to reconstruct rBF in 3D. The reconstructed image from homogeneous phantom and heterogeneous phantom is shown in Figs. 5(a) and 5(b). A reconstructed heterogeneity was clearly recognizable from the overlaid cross-sections compared between the two images. Figure 5(c) shows cross-sectional views of the heterogeneity extracted by half max contrast threshold criteria. The averaged heterogeneity rBF was 0.38 with center (0.0,−0.1,25.0) close to the actual center (0,0,24.5). Reconstructed heterogeneity side length was 7.2 mm with dimensions that were accurate compared to the true solid phantom.

We likewise simulated the phantom experiment by computer using identical parameters. The region with heterogeneity extracted by half max contrast threshold is shown in Fig. 5(d). The reconstructed heterogeneity averaged rBF was 0.37 with center (−0.1,0.0,24.0), similar to phantom results (averaged rBF within 3% of phantom test results). Corresponding 3D flow distributions were also similar to the phantom experiment [Fig. 5(b)] and hence are not shown. We also performed two simulations with off-center locations, but otherwise similar setup, of the heterogeneity and found the reconstructed center and side length in agreement with the expectation.

In this study, an exposure time of 2 ms was selected to achieve a good contrast to noise ratio.[16] The reconstruction and boundary data parameters of delay time τ and window size used herein have been discussed in detail
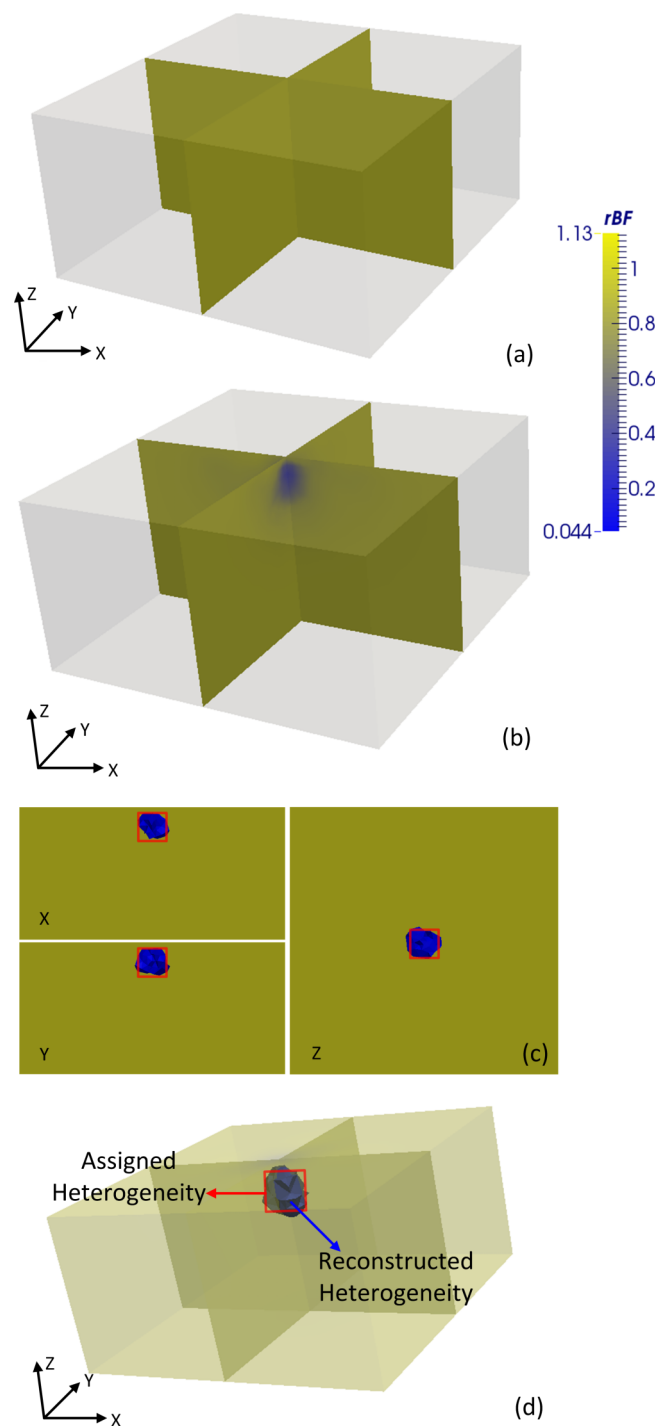
FIG. 5. Reconstructed 3D flow contrasts. Three-dimensional overlaid cross-sectional views of the slab phantom (a) without heterogeneity and (b) with heterogeneity. (c) Two-dimensional cross-sectional view (x and y through side centers; z at 24.5) of the region with heterogeneity as extracted by half max contrast threshold criteria. The true region with heterogeneity is depicted by centered squares. (d) The extracted (half max contrast threshold) region with heterogeneity obtained by computer simulation. Images displayed with ParaView (Kitware, NY).

elsewhere.[5,11] We acknowledge that static scatterer contributions can degrade the current model. Ideally, recovered rBF would be zero. However, we only sought to validate 3D flow contrast detection using our new scDCT method rather than optimize flow recovery accuracy, and we produced

sufficient contrast to identify and characterize the anomalous presence. The agreement between scDCT and DCS on a homogeneous phantom and between simulation and phantom in heterogeneity detection supports success. Furthermore, multiple two-dimensional $S - D$ pairs provided by the CCD omit the probe scanning in ncDCT,[5] and thus significantly improve the spatial and temporal resolution. In addition, due to decreasing signal with increased $S - D$ separation using a point source we were limited to at most 2.2 cm after noise correction. Nevertheless, this $S - D$ separation is still capable of probing tissues ~1 cm depth.

We also note that although the FEM framework allows incorporating complex heterogeneities and boundaries, we chose to exemplify our technique in a straightforward setup. Further difficulties may be encountered when extending scDCT to real complex media. For example, surface curvature may result in modified light distributions and $S - D$ separations potentially reducing the accuracy and reliability of reconstructed flow contrasts. These issues are beyond the scope of the current paper, but can be addressed in the future through computer simulations, possible free-space corrections,[17] and telecentric zoom lens incorporation.[18,19]

4. CONCLUSIONS

We reported a cost-effective CCD-based reflectance 3D flow imaging system from laser speckle contrast with four target-contacted fibers serving as point sources. Beyond dark and shot noise corrections, we successfully incorporated an additional desmearing algorithm. This correction was found to be imperative for reflectance applications using a point source to obtain accurate deep tissue speckle contrast. Flow contrast was extracted using the relationship between a correlation diffusion equation solution and the speckle contrast. A FEM-based DCT framework was employed to reconstruct spatially distributed blood flow. This system was validated using a reflectance-based measurement on a liquid phantom with an internally placed heterogeneity. Compared to our previous ncDCT design,[5] this system demonstrated potential for fast and dense boundary data acquisition and deep tissue hemodynamics tomography translating directly to human studies (e.g., burn/ulcerous tissue flow detection). In future work, quantitative analysis of 3D heterogeneity flow recovery accuracies with arbitrary tissue boundaries will be performed by computer simulations and phantom tests followed by *in vivo* validation.

[a]C. Huang and D. Irwin contributed equally to this work.
[b]Electronic mail: guoqiang.yu@uky.edu

[1] Y. Lin, L. He, Y. Shang, and G. Yu, "Noncontact diffuse correlation spectroscopy for noninvasive deep tissue blood flow measurement," J. Biomed. Opt. **17**, 010502 (2012).

[2] G. Yu, "Diffuse correlation spectroscopy (DCS): A diagnostic tool for assessing tissue blood flow in vascular-related diseases and therapies," Curr. Med. Imaging Rev. **8**, 194–210 (2012).

[3] D. A. Boas and A. G. Yodh, "Spatially varying dynamical properties of turbid media probed with diffusing temporal light correlation," J. Opt. Soc. Am. A **14**, 192–215 (1997).

[4] C. Zhou, G. Yu, D. Furuya, J. H. Greenberg, A. G. Yodh, and T. Durduran, "Diffuse optical correlation tomography of cerebral blood flow during cortical spreading depression in rat brain," Opt. Express **14**, 1125–1144 (2006).

[5] Y. Lin, C. Huang, D. Irwin, L. He, Y. Shang, and G. Yu, "Three-dimensional flow contrast imaging of deep tissue using noncontact diffuse correlation tomography," Appl. Phys. Lett. **104**, 121103 (2014).

[6] H. Dehghani, M. E. Eames, P. K. Yalavarthy, S. C. Davis, S. Srinivasan, C. M. Carpenter, B. W. Pogue, and K. D. Paulsen, "Near infrared optical tomography using NIRFAST: Algorithm for numerical model and image reconstruction," Commun. Numer. Methods Eng. **25**, 711–732 (2008).

[7] A. F. Fercher and J. D. Briers, "Flow visualization by means of single-exposure speckle photography," Opt. Commun. **37**, 326–330 (1981).

[8] R. Bi, J. Dong, and K. Lee, "Deep tissue flowmetry based on diffuse speckle contrast analysis," Opt. Lett. **38**, 1401–1403 (2013).

[9] C. P. Valdes, H. M. Varma, A. K. Kristoffersen, T. Dragojevic, J. P. Culver, and T. Durduran, "Speckle contrast optical spectroscopy, a non-invasive, diffuse optical method for measuring microvascular blood flow in tissue," Biomed. Opt. Express **5**, 2769–2784 (2014).

[10] H. M. Varma, C. P. Valdes, A. K. Kristoffersen, J. P. Culver, and T. Durduran, "Speckle contrast optical tomography: A new method for deep tissue three-dimensional tomography of blood flow," Biomed. Opt. Express **5**, 1275–1289 (2014).

[11] D. A. Boas and A. K. Dunn, "Laser speckle contrast imaging in biomedical optics," J. Biomed. Opt. **15**, 011109 (2010).

[12] R. Bandyopadhyay, A. S. Gittings, S. S. Suh, P. K. Dixon, and D. J. Durian, "Speckle-visibility spectroscopy: A tool to study time-varying dynamics," Rev. Sci. Instrum. **76**, 093110 (2005).

[13] W. Ruyten, "Smear correction for frame transfer charge-coupled-device cameras," Opt. Lett. **24**, 878–880 (1999).

[14] S. Yuan, "Sensitivity, noise and quantitative model of laser speckle contrast imaging," Ph.D. thesis, Tufts University, MA, 2008.

[15] D. Irwin, L. Dong, Y. Shang, R. Cheng, M. Kudrimoti, S. D. Stevens, and G. Yu, "Influences of tissue absorption and scattering on diffuse correlation spectroscopy blood flow measurements," Biomed. Opt. Express **2**, 1969–1985 (2011).

[16] S. Yuan, A. Devor, D. A. Boas, and A. K. Dunn, "Determination of optimal exposure time for imaging of blood flow changes with laser speckle contrast imaging," Appl. Opt. **44**, 1823–1830 (2005).

[17] J. Ripoll, R. B. Schulz, and V. Ntziachristos, "Free-space propagation of diffuse light: Theory and experiments," Phys. Rev. Lett. **91**, 103901 (2003).

[18] L. Zhang, H. Zhao, W. B. Dong, N. Cao, and P. F. Zhang, "Design of an optical system consisting of a special telecentric lens for side-scattering measurement on individual cells," Opt. Eng. **49**, 053001 (2010).

[19] M. Watanabe and S. K. Nayar, "Telecentric optics for focus analysis," IEEE Trans. Pattern Anal. Mach. Intell. **19**, 1360–1365 (1997).